Constraints on the quasi-normal mode frequencies of the LIGO-Virgo signals by making full use of gravitational-wave modeling

Abhirup Ghosh,[1] Richard Brito,[2] and Alessandra Buonanno[1,3]

[1]*Max Planck Institute for Gravitational Physics (Albert Einstein Institute), Am Mühlenberg 1, Potsdam 14476, Germany*
[2]*Dipartimento di Fisica, "Sapienza" Università di Roma & Sezione INFN Roma1, Piazzale Aldo Moro 5, 00185 Roma, Italia*
[3]*Department of Physics, University of Maryland, College Park, MD 20742, USA*

(Dated: January 25, 2021)

The no-hair conjecture in General Relativity states that the properties of an astrophysical Kerr black hole (BH) are completely described by its mass and spin angular momentum. As a consequence, the complex quasi-normal-mode (QNM) frequencies of a binary black hole (BBH) ringdown can be uniquely determined by the mass and spin of the remnant object. Conversely, measurement of the QNM frequencies could be an independent test of the no-hair conjecture. This paper extends to spinning BHs earlier work that proposed to test the no-hair conjecture by measuring the complex QNM frequencies of a BBH ringdown using inspiral-merger-ringdown waveforms, thereby taking full advantage of the entire signal power and removing dependency on the predicted or estimated start time of the proposed ringdown. We further demonstrate the robustness of the test against modified gravitational-wave (GW) signals with a ringdown different from what GR predicts for Kerr BHs. Our method was used to analyse the properties of the merger remnants for the events observed by LIGO-Virgo in the first half of their third observing run (O3a) in the latest LIGO-Virgo publication. In this paper, for the first time, we analyse the GW events from the first (O1) and second (O2) LIGO-Virgo observing runs and provide joint constraints with published results from O3a. We also analyse two events from the O3a catalogue that were not considered in the initial LIGO-Virgo analysis. The joint measurements of the fractional deviations in the frequency and damping time, $\delta f_{220} = XX\pm$ and $\delta\tau_{220} = YY\pm$ are the strongest constraints yet using this method.

I. INTRODUCTION

[AB: Please make the citations in the bibliography uniform (I would stick with citations taken from InSpires and remove the URL links). We will be submitting to Physical Review D, so please stick with American English. Also, please be uniform when writing captions, when using colors and style of curves in plots, when building Tables. There is not a lot of discussion in the text on the main results of the paper (Sec. IV). The abstract would need to be tighten and made more crispy once the quantitative results for the bounds are included.]

The LIGO Scientific Collaboration [1] and the Virgo Collaborations [2] have recently announced their catalogue of gravitational-wave (GW) observations signals [**?**] from the first half of their third observing run (O3a) [**?**]. Combined with the confirmed observations from the first and second observing-run catalogues [3], the Advanced LIGO detectors at Hanford, Washington and Livingston, Louisiana [4], and the Advanced Virgo detector in Cascina, Italy [5] have now detected more than 50 GW events from the merger of compact objects like neutron stars and/or black holes (BHs)., collectively called compact binary coalescences (CBCs). Alongside independent claims of detections [6–10], this these results has have firmly established the field of GW astronomy, five years on from after the first ever direct detection of a GW passing through the on Earth, notably GW150914 on September 14,2015 [11].

The observation of GWs has had significant astrophysical and cosmological implications [12–15]. It has also allowed us to make statements in probe fundamental physics .Specifically, LIGO-Virgo's observations have allowed us to and test predictions of Einstein's theory of General Relativity (GR) [**?**] in the previously unexplored highly-dynamical, and strong field regime of highly relativistic, strong-field regimes of gravity [16–18]. In GR, a CBC involving two BHs (a binary black hole (BBH) system) is described in by three distinct phases: an early *inspiral*, where the two compact objects spiral in loosing energy because of the emission of GWs and *plunge* due to a back-reaction of GW-emission, a *merger* marked by the formation of an common apparent horizon [**?**], and a late-time *ringdown*, where during which the newly formed remnant object settles down to a stable Kerr BH state through the emission of emitting an exponentially damped quasi-normal-modes (QNMs) spectrum of gravitational radiation [**? ?**] (i.e., damped oscillations with specific, discrete frequencies and decay times).

The LIGO-Virgo collaborations have released companion papers [] detailing their latest results of tests of GR using events for GW150914 [] and for several GW events of the first two transient catalogues (TC): GWTC-1[] and GWTC-2 []. The results include tests of GW generation and source dynamics, where bounds are placed on parameterized deviations in the post-Newtonian (PN) coefficients describing the early inspiral [**?**], and phenomenological coefficients describing the intermediate (plunge) and merger regimes of coalescence [**?**]; tests of GW propagation, which assume a generalized dispersion relation and place upper bounds on the Compton wavelength and, consequently, the mass of the graviton [19, 20], and tests of the polarization of gravitational radiation using a multi–GW-detector network [21, 22]. The GWTC-1/2 papers also checks for consistency between different portions of the signal using estimates of for the predicted mass and spin of the remnant object [16, 23, 24], and consistency of the residuals with interferometric noise [18, 25]. None of these tests report any departure from the predictions of GR.

The first paper on tests of GR by the LIGO Collaboration [] provided us with the first measurement of the dominant damped-oscillation signal in the ringdown stage of a

BBH coalescence. The LIGO-Virgo O3a testing GR paper [] has recently reported ~~also details results on tests~~ a comprehensive analysis of the properties of the remnant object, including the ringdown stage, for tens of GW events. ~~BH ringdown and nature of the remnant object, which is an active field of research at the moment.~~ The no-hair conjecture in GR [] states that an (electrically neutral) astrophysical BH is completely described by two observables: mass and spin angular momentum. One consequence of the no-hair conjecture is that the (complex) QNM frequencies of gravitational radiation emitted by a perturbed isolated BH are ~~is~~ uniquely determined by its mass and spin angular momentum. Hence a test of the no-hair conjecture would involve checking for consistency between estimates of mass and spin of the remnant object across multiple QNM frequencies [**?**]. An inconsistency would either indicate a non-BH nature of the remnant object, or an incompleteness of GR as the underlying theory of gravity.

The consistency between the post-merger signal and the least damped QNM was first demonstrated in Ref. [16] for GW150914, and later extended to include overtones in Refs. [26–30]. Consistency of the late-time ~~signal~~ waveform with a single QNM is a test of the ringdown of a BBH coalescence, but not necessarily a test of the no-hair conjecture, which requires the measurement of (at least) two QNMs (BH spectroscopy), and ~~checking for~~ consistency between them [31**?**]. Recent work in that direction [AB: which direction? There are papers by Nikhef group and also Brito et al., and many others that have investigated BH spectroscopy.] include [32–34]. The nature of the remnant object has also been explored through tests of BH thermodynamics, like the Hawking's area theorem [35] or through search for echos in the post-merger signal [36–41]. None of these tests have found evidence for non-BH nature of the remnant object (as described in GR) in LIGO-Virgo BBH observations.

[AB: I don't understand the next sentence, it looks to me out of context.] Most of the tests mentioned above focus on analysing the post-merger or late-time ringdown signal in isolation. ~~Second generation ground-based interferometric detectors like~~ Ground-based detectors, such as ~~Advanced~~ LIGO and Virgo, are most sensitive to stellar-mass BH binaries that merge near the minimum~~a~~ of their sensitivity band ($\sim$ 100Hz). As a consequence, the remnant object *rings down* [AB: we are not discussing the interferometer noises, so why to give such a detail about the shot noise?] ~~in shot-noise dominated higher frequencies, leaving~~ at frequencies where the sensitivity is worse, leaving very little signal-to-noise ratio (SNR) in the post-merger signal. [AB: This discussion about the starting time of the ringdown starts too abruptly, and looks out of context and incomplete. Also, why are we citing only those papers? The matter has a long history. There have been calibrations to NR of damped- oscillation signals.] The ringdown start time is not a clearly defined quantity and has been explored in detail in Ref. [42]. In other works [32, 33], it has been left as a free parameter to be estimated directly from the data. Uncertainties in estimates of the ringdown start-time, as well as, an overall lack of SNR in the post-merger signal, given typical sensitivities of ground-based detectors, result in significant statistical uncertainties in the measurement of the QNM frequencies.

An independent approach to BH spectroscopy, based on the full-signal analysis, was ~~outlined~~ introduced in Ref. [26] (henceforth referred to as Paper I). Unlike methods that focus only on the post-merger signal, it ~~describes a framework in which a~~ employs the complete inspiral-merger-ringdown (IMR) waveform ~~model is used~~ to measure the complex QNM frequencies. This ~~allows~~ gives access to the full SNR of the signal, reducing measurement uncertainties. Moreover, the definition of the ringdown start time is built into the merger-ringdown model and does not need to be either left as an additional free parameter or fixed using alternate definitions. While Paper I presented the method and tested it for ~~in the context of a non-spinning waveform model~~ non-spinning BBHs, here we extend the analysis to the more realistic astrophysical case in which BHs carry spins~~ in the current paper~~. Furthermore, the IMR waveform model used in this paper is more accurate than what employed in Paper I, because it contains higher-order corrections in PN theory and it was calibrated to a much larger set of numerical-relativity (NR) waveforms [43]. All astrophysical BHs are expected to be spinning, and ignoring effects of spin has been shown to introduce systematic biases in the measurement of the source properties [**?**].

The rest of the paper is organized as follows. Section I describes our parameterized IMR waveform model. In Sec. I, we define our framework to test GR, notably how we can measure complex QNM frequencies with our parameterized model within a Bayesian formalism. Then, in Sec. I, we demonstrate our method on real GW events, as well as simulated signals. In particular, we analyze the ... and constrain the QNM frequecies ... Finally, in Sec. V we provide a summary of our results and discuss future developments.

II. WAVEFORM MODEL AND STATISTICAL STRATEGY TO MEASURE QUASI-NORMAL MODES

[AB: In the following, I will not use much the strike-out, but instead I will bracket in color the text that I have changed.]

A GW signal from the (quasi-circular) coalescence of two BHs is completely described in GR by a ~~fixed set of~~ 15 parameters, $\boldsymbol{\xi}_{\rm GR}$. These can be grouped into the *intrinsic* parameters: the masses, m_1, m_2 and spins, $\vec{\boldsymbol{S}}_{\boldsymbol{1}}, \vec{\boldsymbol{S}}_{\boldsymbol{2}}$ of the component objects in the ~~initial~~ binary; and the *extrinsic* parameters: a reference time t_c and phase ϕ_c, the sky position of the binary (α, δ), the luminosity distance, d_L, and the binary's orientation described through the inclination of the binary ι and its polarization ψ. We also introduce the total mass $M = m_1 + m_2$, and the (dimensionless) symmetric mass ratio $\nu = m_1 m_2 / M^2$.

Here, we focus on BHs with spins aligned or anti-aligned with the orbital angular momentum (henceforth, "aligned-spin"). In this case, the GW signal depends on 11 parameters. We denote the aligned-spin (dimensionless) components as $\chi_i = |\vec{S}_i|/m_i^2$, where $i = 1, 2$ for the two BHs.

A. Parameterized waveform model

As in Paper I, we use an IMR waveform model developed within the effective-one-body (EOB) formalism []. However, whereas Paper I was limited to non-spinning multipolar waveforms, here we use as our baseline model the aligned-spin multipolar waveform model developed in Ref. [44]. In addition to being calibrated to NR simulations, this model also uses information from BH perturbation theory for the merger and ringdown phases. ~~Therefore this waveform model provides a very accurate and faithful semi-analytic description of the inspiral, merger and ringdown phases.~~ Henceforth we will denote this model by SEOBNR for short [1].

In the observer's frame, the GW polarizations can be written as

$$h_+(\iota,\varphi;t) - i h_\times(\iota,\varphi;t) = \sum_{\ell,m} {}_{-2}Y_{\ell m}(\iota,\varphi)\, h_{\ell m}(t)\,, \tag{2.1}$$

[AB: there is a mismatch of notations for the parameters with respect to what was introduced above.] where φ is the azimuthal direction to the observer, ${}_{-2}Y_{\ell m}(\theta,\varphi)$ are the -2 spin-weighted spherical harmonics. The SEOBNR model we employ includes the $(\ell,|m|) = (2,2),(2,1),(3,3),(4,4)$, and $(5,5)$ modes [44]. For each (ℓ,m), the inspiral-(plunge-)merger-ringdown SEOBNR waveform is schematically given by

$$h_{\ell m}(t) = h^{\rm insp-plunge}_{\ell m}\,\theta(t^{\ell m}_{\rm match}-t) + h^{\rm merger-RD}_{\ell m}\,\theta(t-t^{\ell m}_{\rm match})\,, \tag{2.2}$$

where $\theta(t)$ is the Heaviside step function, $h^{\rm insp-plunge}_{\ell m}$ represents the inspiral-plunge part of the waveform, whereas $h^{\rm merger-RD}_{\ell m}$ denotes the merger-ringdown waveform, which reads [43, 44]

$$h^{\rm merger\text{-}RD}_{\ell m}(t) = \nu\,\tilde{A}_{\ell m}(t)\, e^{i\tilde{\phi}_{\ell m}(t)}\, e^{-i\sigma_{\ell m0}(t-t^{\ell m}_{\rm match})}, \tag{2.3}$$

where ν is the symmetric mass ratio of the binary and $\sigma_{\ell m0} = 2\pi f_{\ell m0} - i/\tau_{\ell m0}$ denotes the complex frequency of the fundamental QNMs of the remnant BH. We denote the oscillation frequencies by $f_{\ell m0} \equiv \Re(\sigma_{\ell m0})/(2\pi)$ and the decay times by $\tau_{\ell m0} \equiv -1/\Im(\sigma_{\ell m0})$. The functions $\tilde{A}_{\ell m}(t)$ and $\tilde{\phi}_{\ell m}(t)$ are given by [43, 44]:

$$\tilde{A}_{\ell m}(t) = c^{\ell m}_{1,c}\tanh[c^{\ell m}_{1,f}\,(t-t^{\ell m}_{\rm match}) + c^{\ell m}_{2,f}] + c^{\ell m}_{2,c}, \tag{2.4}$$

$$\tilde{\phi}_{\ell m}(t) = \phi^{\ell m}_{\rm match} - d^{\ell m}_{1,c}\log\left[\frac{1+d^{\ell m}_{2,f}e^{-d^{\ell m}_{1,f}(t-t^{\ell m}_{\rm match})}}{1+d^{\ell m}_{2,f}}\right], \tag{2.5}$$

where $\phi^{\ell m}_{\rm match}$ is the phase of the inspiral-plunge mode (ℓ,m) computed at $t = t^{\ell m}_{\rm match}$. The coefficients $d^{\ell m}_{1,c}$ and $c^{\ell m}_{i,c}$ with $i = 1,2$ are fixed by imposing that the functions $\tilde{A}_{\ell m}(t)$ and $\tilde{\phi}_{\ell m}(t)$ are of class C^1 at $t = t^{\ell m}_{\rm match}$, when matching the merger-ringdown waveform to the inspiral-plunge SEOBNR waveform $h^{\rm inspiral-plunge}_{\ell m}(t)$. This allows us to write the coefficients $c^{\ell m}_{i,c}$ as [44]:

$$\begin{aligned} c^{\ell m}_{1,c} = \frac{1}{c^{\ell m}_{1,f}\nu}\big[&\partial_t|h^{\rm insp\text{-}plunge}_{\ell m}(t^{\ell m}_{\rm match})| \\ &- \sigma^{\rm R}_{\ell m}|h^{\rm insp\text{-}plunge}_{\ell m}(t^{\ell m}_{\rm match})|\big]\cosh^2(c^{\ell m}_{2,f}), \end{aligned} \tag{2.6}$$

$$\begin{aligned} c^{\ell m}_{2,c} = -\frac{|h^{\rm insp\text{-}plunge}_{\ell m}(t^{\ell m}_{\rm match})|}{\nu} + \frac{1}{c^{\ell m}_{1,f}\nu}\big[&\partial_t|h^{\rm insp\text{-}plunge}_{\ell m}(t^{\ell m}_{\rm match})| \\ &- \sigma^{\rm R}_{\ell m}|h^{\rm insp\text{-}plunge}_{\ell m}(t^{\ell m}_{\rm match})|\big]\cosh(c^{\ell m}_{2,f})\sinh(c^{\ell m}_{2,f}), \end{aligned} \tag{2.7}$$

and $d^{\ell m}_{1,c}$ as

$$d^{\ell m}_{1,c} = \left[\omega^{\rm insp\text{-}plunge}_{\ell m}(t^{\ell m}_{\rm match}) - \sigma^{\rm I}_{\ell m}\right]\frac{1+d^{\ell m}_{2,f}}{d^{\ell m}_{1,f}d^{\ell m}_{2,f}}\,, \tag{2.8}$$

where we denoted $\sigma^{\rm R}_{\ell m} \equiv \Im(\sigma_{\ell m0}) < 0$ and $\sigma^{\rm I}_{\ell m} \equiv -\Re(\sigma_{\ell m0})$, and $\omega^{\rm insp\text{-}plunge}_{\ell m}(t)$ is the frequency of the inspiral-plunge EOB mode. The coefficients $c^{\ell m}_{i,f}$ and $d^{\ell m}_{i,f}$ are obtained through fits to NR and Teukolsky-equation–based waveforms and can be found in Appendix C of Ref. [44].

In the SEOBNR model constructed in Ref. [44], the complex frequencies $\sigma_{\ell m0}$ are expressed in terms of the final BH mass and spin [31, 45], and the latter are related to the BBH's component masses and spins through NR–fitting-formulas obtained in GR [46, 47]. Here instead, in the spirit of what was done in Paper I, we promote the QNM (complex) frequencies to be free parameters of the model, while keeping the inspiral-plunge modes $h^{\rm inspiral-plunge}_{\ell m}(t)$ fixed to their GR values. More explicitly, we introduce a parameterized version of the SEOBNR model where the frequency and the damping time of the $\ell m0$ mode (i.e, $(f_{\ell m0},\tau_{\ell m0})$) is defined through the fractional deviations, $(\delta f_{\ell m0},\delta\tau_{\ell m0})$, from the corresponding GR values, which are obtained using NR fits [46, 47]. Thus,

$$f_{\ell m0} = f^{\rm GR}_{\ell m0}\,(1+\delta f_{\ell m0})\,, \tag{2.9}$$

$$\tau_{\ell m0} = \tau^{\rm GR}_{\ell m0}\,(1+\delta\tau_{\ell m0})\,. \tag{2.10}$$

We denote such a parameterized waveform model pSEOBNR [2].

As said, the GR quantities $(f^{GR}_{\ell m0},\tau^{GR}_{\ell m0})$ are constructed using the same NR–fitting–formula ~~prescriptiion~~ described above. We note that when leaving $\sigma_{\ell m}$ to vary freely, the functions $\tilde{A}_{\ell m}(t)$ and $\tilde{\phi}_{\ell m}(t)$ ~~will~~ in general also differ from the GR predictions, since those functions depend on the QNM complex frequencies, as can be seen from the expressions for $c^{\ell m}_{i,c}$ and $d^{\ell m}_{1,c}$ in Eqs. (2.6), (2.7), and (2.8).

B. Bayesian parameter-estimation technique

The parameterized model, pSEOBNR, described above introduces an additional set of non-GR parameters, $\boldsymbol{\xi}_{\rm nGR}$ =

[1] In the LIGO Algorithm Library (LAL), this waveform model is called SEOBNRv4HM.

[2] This waveform model is called pSEOBNRv4HM in LAL.

$(\delta f_{\ell m0}, \delta\tau_{\ell m0})$, corresponding to each (ℓ, m) QNM present in the GR waveform model `SEOBNR`. One then proceeds to use the Bayes theorem to obtain the *posterior* probability distribution on $\boldsymbol{\lambda} = \{\boldsymbol{\xi}_{\rm GR}, \boldsymbol{\xi}_{\rm nGR}\}$, given a hypothesis $\mathcal{H}$:

$$P(\boldsymbol{\lambda}|d,\mathcal{H}) = \frac{P(\boldsymbol{\lambda}|\mathcal{H})\,\mathcal{L}(d|\boldsymbol{\lambda},\mathcal{H})}{P(d|\mathcal{H})}, \tag{2.11}$$

where $P(\boldsymbol{\lambda}|\mathcal{H})$ is the *prior* probability distribution, and $\mathcal{L}(d|\boldsymbol{\lambda},\mathcal{H})$ is called the *likelihood* function. The denominator is a normalization constant $P(d|\mathcal{H}) = \int P(\boldsymbol{\lambda}|\mathcal{H})\,\mathcal{L}(d|\boldsymbol{\lambda},\mathcal{H})\,d\boldsymbol{\lambda}$, called the marginal likelihood, or the *evidence* of the hypothesis $\mathcal{H}$. In this case, our hypothesis $\mathcal{H}$ is that the data contains a GW signal that is described by the `pSEOBNR` waveform model $h(\boldsymbol{\lambda})$ and stationary Gaussian noise described by a power spectral density (PSD) $S_n(f)$. The likelihood function can consequently be defined as:

$$\mathcal{L}(d|\boldsymbol{\lambda},\mathcal{H}) \propto \exp\big[-\frac{1}{2}\langle d-h(\boldsymbol{\lambda})\,|\,d-h(\boldsymbol{\lambda})\rangle\big], \tag{2.12}$$

where $\langle .|. \rangle$ is the following noise-weighted inner product:

$$\langle A|B\rangle = \int_{f_{\rm low}}^{f_{\rm high}} df \frac{\tilde{A}^*(f)\tilde{B}(f) + \tilde{A}(f)\tilde{B}^*(f)}{S_n(f)}. \tag{2.13}$$

The quantity $\tilde{A}(f)$ denotes the Fourier transform of $A(t)$ and the * indicates complex conjugation. The limits of integration $f_{\rm low}$ and $f_{\rm high}$ define the bandwidth of the sensitivity of the GW detector. We usually assume $f_{\rm high}$ to be the Nyquist frequency whereas $f_{\rm low}$ is dictated by the performance of the GW detector at low-frequency and we assume XXX. [AB: It isn't just seismic noise. In fact, at low frequency, there are mysterious noises that people have had hard time to control.] ~~the response of the gravitational detector to low-frequency seismic noise.~~ Owing to the large dimensionality of the parameter set $\boldsymbol{\lambda}$, the posterior distribution $P(\boldsymbol{\lambda}|d,\mathcal{H})$ in Eq. (2.11) is computed by stochastically sampling the parameter space using techniques such as Markov-chain Monte Carlo (MCMC) [] or Nested Sampling []. For this paper, we use the `LALInference` [] and `Bilby` codes [] that provide an implementation of the parallely tempered MCMC and Nested Sampling algorithms respectively, for computing the posterior distributions.

Given the full-dimensional posterior probability density function $P(\boldsymbol{\lambda}|d,\mathcal{H})$, we can marginalize over the *nuisance* parameters, to obtain the marginalized posterior probability density function over the QNM parameters $\boldsymbol{\xi}_{\rm nGR}$:

$$P(\boldsymbol{\xi}_{\rm nGR}|d,\mathcal{H}) = \int P(\boldsymbol{\lambda}|d,\mathcal{H}) d\boldsymbol{\xi}_{\rm GR}\,. \tag{2.14}$$

For most of the results discussed in this paper, we restrict ourselves to the $(\ell m) = (2,2)$ and/or $(3,3)$ modes. In those cases we ~~would~~ assume $\boldsymbol{\xi}_{\rm nGR} = \{\delta f_{220}, \delta\tau_{220}\}$ and/or $\{\delta f_{330}, \delta\tau_{330}\}$, and all the other (ℓm) modes to be fixed at their GR predictions (i.e., $\delta f_{\ell m0} = \delta\tau_{\ell m0} = 0$). This is because, for most of the high-mass BH events that we find most appropriate for this test, the LIGO-Virgo observations are consistent with nearly–equal-mass face-on/off BBHs for which power in the subdominant modes is not enough to attempt to measure more than one, or at most [AB: it seems some wrods are missing to make the senetence meaningful] QNM frequencies, simultaneously.

Lastly, throughout our analysis, we assume uniform priors on our non-GR QNM parameters, $(\delta f_{\ell m0}, \delta\tau_{\ell m0})$. However, since the priors on $(f^{GR}_{\ell m0}, \tau^{GR}_{\ell m0})$ are derived through NR–fits, from the corresponding priors on the initial masses and spins, this leads to a non-trivial prior on the final reconstructed frequency and damping time, $(f_{\ell m0}, \tau_{\ell m0})$. Also, given the definition of the damping time in Sec. I, we ~~realize~~ note that $\delta\tau_{\ell m0} = -1$ leads to the imaginary part of the frequency going to infinity. We avoid this by restricting the minimum of the prior on $\delta\tau_{\ell m0}$ to be greater than -1.

III. SYNTHETIC-SIGNAL INJECTION STUDY

A. Simulations using GR signals in Gaussian noise

We demonstrate our method using synthetic-signal injections describing GWs from BBHs in GR. We employ coloured Gaussian noise with PSDs expected for LIGO and Virgo detectors at design sensitivities []. [AB: Please cite which PSD you used.] For the mock BBH signals, we choose parameters similar to two specific GW events, GW150914 [] and GW190521 []. We list them in Table I. These two binary systems are representative of the kind of systems for which the QNM measurement is most suitable, notably high-mass BBH events which are loud enough that the pre- and post-merger SNRs return reliable parameter-estimation results.

Event	$m_{1,\rm det}(M_\odot)$	$m_{2,\rm det}(M_\odot)$	χ_1	χ_2	SNR
GW150914-like	39	31	0.0	0.0	25
GW190521-like	150	120	0.02	-0.39	14
SXS:BBH:0166	72	12	0.0	0.0	75

TABLE I. Parameters of the synthetic-signal injections, chosen to be similar to the actual GW events indicated in the first column. The parameters $(m_{1,\rm det}, m_{2,\rm det})$ are the detector-frame masses of the primary and secondary BHs, respectively. [AB: I would suggest to give in the Table also the SNR in the pre- and post-merger stages. The third row is completely ignored in the caption's explanations.]

[AB: Nothing is said in the text and the caption of the Table about the third mock signal in the Table!]

To avoid possible systematic biases in our parameter-estimation analysis due to error in waveform modeling, we use the GR version of the same waveform, `SEOBNR` (without allowing for deviations in the QNM parameters) to simulate our GW signal. And to avoid systematic biases due to noise, we use an averaged (zero-noise) realization of the noise. A detailed study on noise systematics for one of the GW events is presented in Appendix A. [AB: This reference to the Appendix is out of context. Why should the reader appreciate at this stage of the paper, where we have not yet discussed results with real data, what is in the Appendix?] As in the case

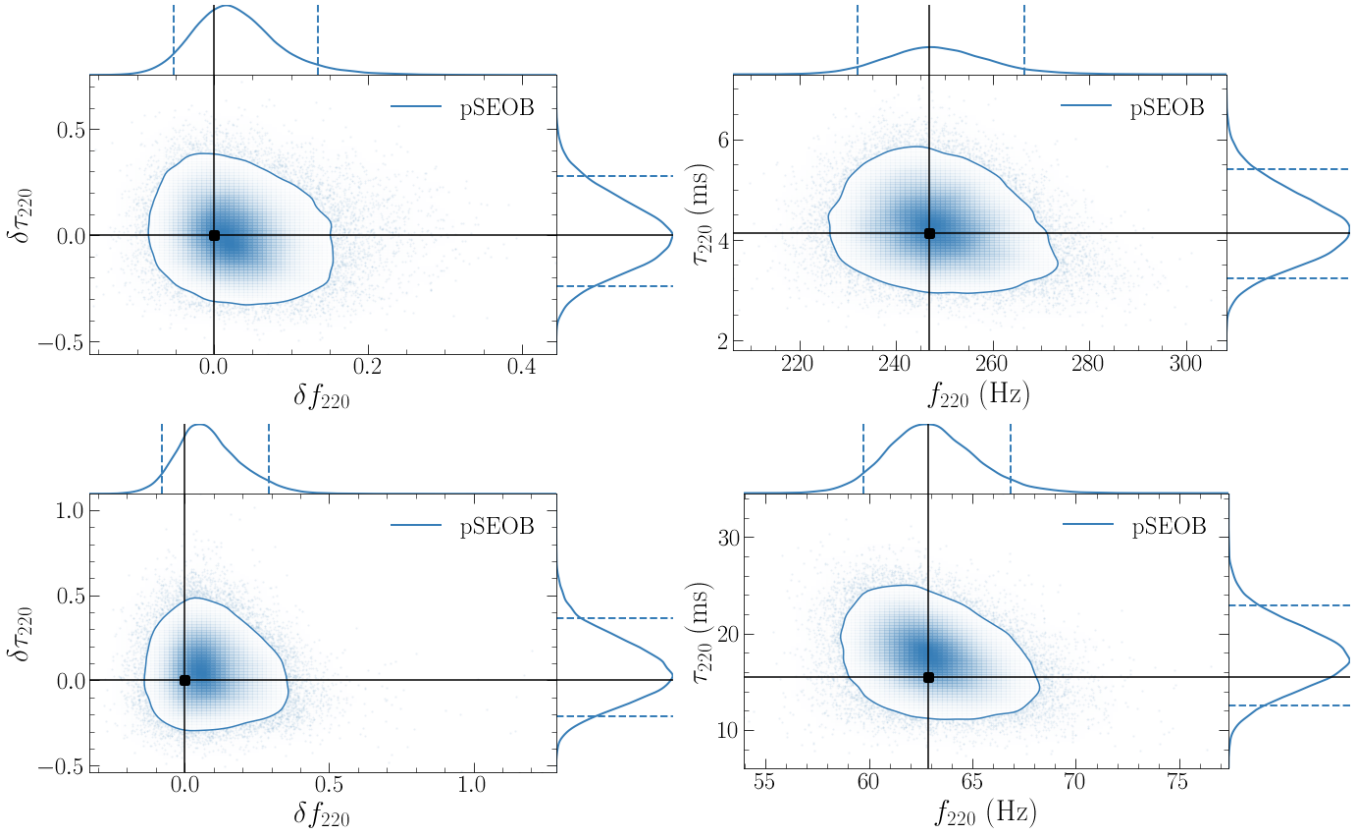

FIG. 1. FINAL RESULT Posterior probability distribution on the fractional deviations in the frequency and damping time of the $(2,2)$ QNM, $(\delta f_{220}, \delta\tau_{220})$ (left panels) and the reconstructed quantities, (f_{220}, τ_{220}) (right panels) for GR injections with initial parameters similar to GW150914 (top panels) and GW190521 (bottom panels) (Table I). The 2D contour marks the 90% credible region, while the dashed lines on the 1D marginalized distributions mark the 90% credible levels. The black vertical and horizontal lines mark the injection values. [AB: Please indicate on the figures: GW150914-like and GW190521-like.] [AB: Please be consistent and use the label pSEOBNR, as in the text, instead of pSEOB.]

of the actual detections, we consider a two-detector LIGO network at Hanford and Livingston, having identical PSDs. The distance to the two synthetic events is rescaled such that the SNR in the detector network is the same as the actual events (i.e., 24 for GW150914 and 14 for GW190521). Since mearly–equal-mass binaries like GW150914 and GW190521 observed at moderately high SNRs are not expected to have a loud ringdown signal, we restrict ourselves to estimating the frequency and damping time of only one QNM $(\ell m) = (2,2)$, i.e., $\{\delta f_{220}, \delta\tau_{220}\}$, while fixing the other QNM frequencies to their GR values.

We find, as one might expect, that the posterior distribution on the parameters describing fractional deviations in the frequency and damping time are consistent with zero (left panels of Fig. 1). One can then convert these fractional quantities into absolute quantities using the relations given in Eqs. 2.9 and 2.10, and construct posterior distributions on these effective quantities, (f_{220}, τ_{220}) (right panels of Fig. 1). In each of these cases, the recovered 2D posteriors are consistent with the GR predictions (black ~~solid lines~~ dot). [AB: please be precise in referring to 1D and 2D posteriors when discussing the figures.]

B. Simulations using non-GR signals in Gaussian noise

To demonstrate the robustness of the method in detecting possible deviations ~~of the underlying GW signal from predictions of~~ from GR, we inject ~~simulated~~ synthetic GW signals which are identical to the corresponding GR prediction up to merger, and differ in their post-merger description. We again choose ~~systems with initial~~-binary-parameters similar to GW150914 and GW190521 (as given in Table XXX), but ~~we attach a phenomenological post-merger signal described by deviation parameters~~ set $\delta f_{220} = \delta\tau_{220} = 0.5$ [AG: deviations=0.1 runs are ongoing and almost done. AB: I would show results that include the 10% case, which is more realistic, based on QNM predictions in theories of gravity alternative to GR.]. In other words, we assume that the frequency and damping time of our non-GR signal is 1.5 times the corresponding GR prediction, although the pre-merger signal is identical to GR. In Fig. 2 we show ... [AB: Not clear to

me what the next sentence says. Coudl you just clearly refer to thePlease introduce the injected signal and the template, which is used to recover it, and simply say that they belong to the same waveform model.] We also avoid waveform ~~and noise~~ systematic biases by choosing a configuration identical to the simulations described in Sec.III A. We summarize the results of the Bayesian analysis in Fig. 3 where we show the posterior probability distributions for $(\delta f_{220}, \delta\tau_{220})$, or equivalently (f_{220}, τ_{220}). We find that they are consistent with the corresponding values of the injection parameters, indicated by the black solid lines. [AB: Please be more quantitative when explaining the results in the figure. Which black lines are you referring to? In the main 2-D figure the injected signal is a point not a line. I think you are referring to the 1D posteriors, but it needs to be explained.]

We additionally investigate the effects of erroneously assuming that ~~an underlying modified~~ a non-GR signal can be well-described by a GR one. We do this by estimating the parameters of our non-GR signals using the GR waveform model `SEOBNR` instead of the parameterized `pSEOBNR`. [AB: Not clear what the next senetnce wants to say.] In such cases, we run the risk of biased parameter estimates due to an incomplete understanding of the underlying signal. The resulting posterior probability distributions are shown in the right panels of Fig. 3 by the red (GW150914-like) and blue (GW190521-like) curves. The results are interesting and distinctly different for the two events. For the GW150914-like [AB: I would avoid using "modified" GR, but istsead non-GR.] non-GR signal, the measurements of $(f_{220}^{\rm GR}, \tau_{220}^{\rm GR})$ (see top right panel in Fig. 3) are consistent with the $(f_{220}^{\rm GR}, \tau_{220}^{\rm GR})$ measurements for a signal with no deviations from GR (see top right panel in Fig. 1). In other words, if the actual signal had deviations from GR as large as the 50% ~~of the GR prediction~~, the analysis with the GR signal `SEOBNR` would likely have reported *no* deviation from the GR prediction. However in the case of the GW190521-like non-GR signal, a simple GR analysis of the non-GR signal would have yielded measurements distinctly different from either of the two parameterized estimates: with and without deviations. [AB: Not clear to me the next sentence. We are working in Gaussian noise, so why are you referring to the noise as the culprit or the source of difference?] The fact that the GW190521-like signal has a much lower SNR than GW150914-like signal might be a possible reason for the measurement of the final quantities to be more susceptible to noise. A more detailed comparison of the other parameters, like the masses and spins, between an `pSEOBNR` and an `SEOBNR` measurement of a modified GR signal is shown in Fig. 4. [AB: Please comment the figures. What are the main results? What do we deduce?]

C. Test of the no-hair conjecture

Finally, we provide a simple demonstration of a test of the no-hair theorem using our model. As described in the introduction, any test of the no-hair theorem of BHs would need to involve independent measurements of (at least) two different QNMs.

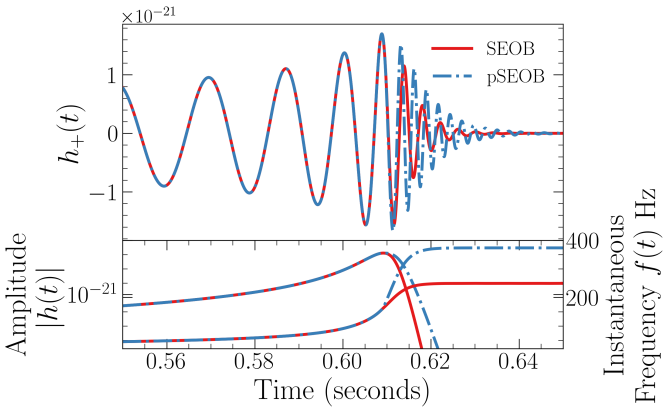

FIG. 2. FINAL RESULT Top panel: The '+'–polarization of the gravitational waveform $h_+(t)$ from a GW150914-like event where the post-merger is described by GR ~~(solid orange lines)~~ (i.e., $\delta f_{220} = \delta\tau_{220} = 0$), and where the merger-ringdown is modified ~~(dashed grey lines)~~ (i.e., $\delta f_{220} = \delta\tau_{220} = 0.5$). Bottom panel: Comparison of the evolution of the amplitude (left) and instantaneous frequency (right) for the GR and ~~modified~~ non-GR signal. [AB: Please remove "Amplitudes" and "Instantaneous Frequency" from the y-axis labels, but instead provide explanations in the caption, and use only $f(t)$ as label.]

Here, we use a ~~simulated~~ NR GW signal from the SXS catalog [] corresponding to a non-spinning BBH with mass-ratio $q = 6$ (SXS:BBH:0166), ~~rescaled to a~~ total mass $M = 84M_\odot$ (see Table I). We choose an asymmetric system to increase the SNR in the higher modes. We also ~~rescale~~ choose the distance and orientation of the binary such that the total SNR ~~of the signal~~ in ~~a~~ the network of the three detectors, LIGO Hanford, Livingston and Virgo, is 75. Based on the LIGO-Virgo observations during O3a, such asymmetric and loud signals are no longer just a theoretical prediction, but quite plausible at design sensitivities. Using this signal, we attempt to measure both the ~~QNM frequencies~~ $(2, \pm 2)$ and $(3, \pm 3)$ ~~modes~~ QNMs ~~together~~. We summarize our results in Fig. 5. For this injected signal the SNR in other sub-dominant modes is too low to be able to measure them. ~~less for us to estimate them reliably.~~

The fractional deviations in the estimates of the damping time and frequency of either mode is expected to be consistent with 0, as we indeed find in the left panel of Fig. 5. Consequently we find that the reconstructed quantities (f_{220}, τ_{220}) and (f_{330}, τ_{330}) are also consistent with the corresponding predictions for a BBH merger in GR. As a consequence, the information from these two independent measures correspond to a unique remnant object, which is completely described by its mass and spin angular momentum [*AG: have the mf-af plot as well as a third panel to show consistency*]. For most of the events observed so far, the power in the $(3, \pm 3)$ has not been sufficient to measure it along with the $(2, \pm 2)$, or in fact, in its place. However, it might also be possible to combine information from multiple observation~~, as is likely~~ over the coming few years ~~of GW astronomy with the LIGO-Virgo detectors,~~ to obtain meaningful constraints on the $(3, \pm 3)$ and other sub-dominant QNMs [].

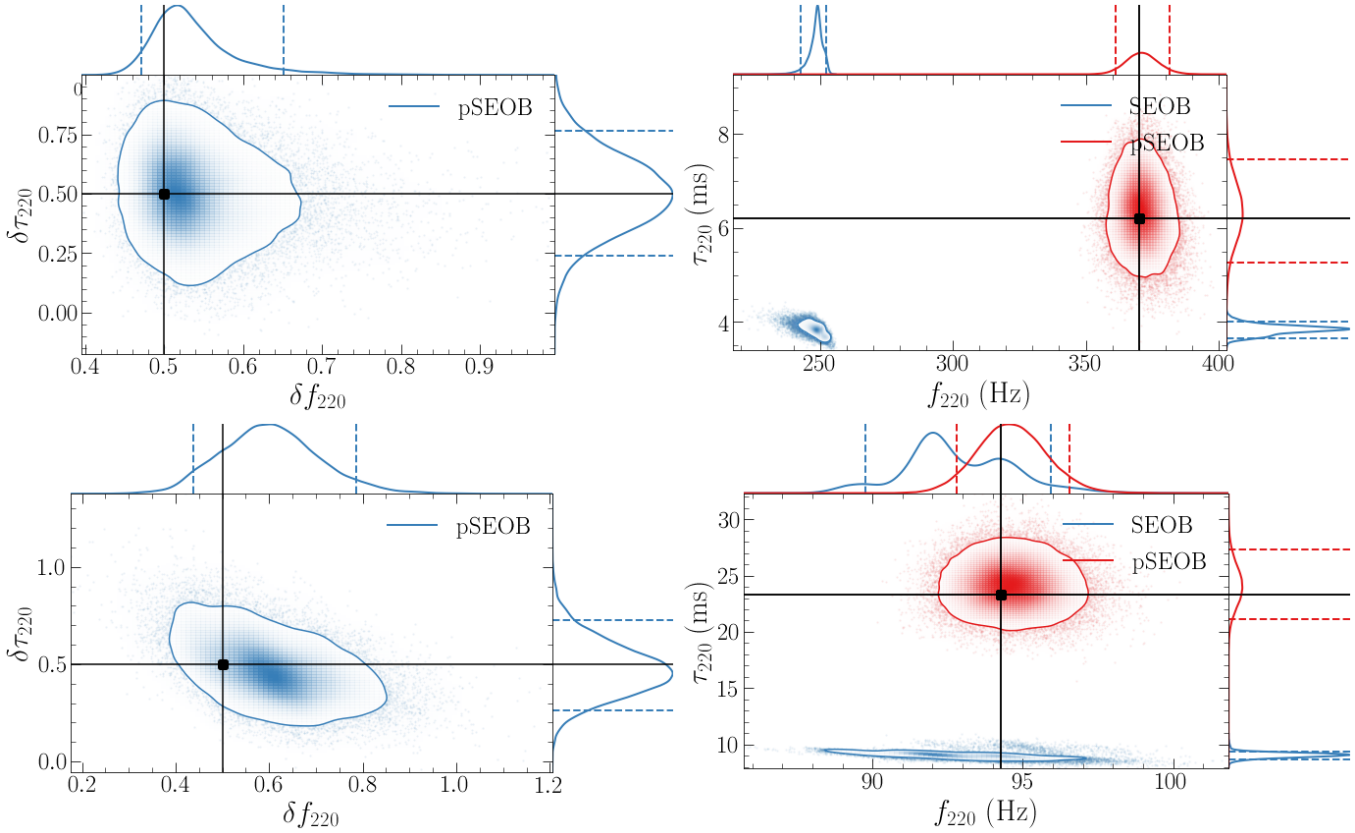

FIG. 3. FINAL RESULT Posterior probability distribution on the fractional deviations in the frequency and damping time of the (2, 2) QNM, $(\delta f_{220}, \delta\tau_{220})$ (left panels) and the reconstructed quantities, (f_{220}, τ_{220}) (right panels) for ~~modGR~~ non-GR injections with ~~initial~~ parameters ~~similar to~~ of GW150914-like (top panels) and GW190521-like (bottom panels) as given in Table I. The ~~underlying~~ non-GR signal has a deviation, $\delta f_{220} = \delta\tau_{220} = XX$. The 2D contour marks the 90% credible region, while the dashed lines on the 1D marginalized distributions mark the 90% credible levels. The black vertical and horizontal lines mark the injection values. In the right panels, we additionally show measurements using a GR (SEOBNR) waveform, for the GW150914-like ~~(grey)~~ (upper panel) and GW190521-like ~~(pink)~~ (lower panel) injections. The measurements with SEOBNR waveforms are visibly biased. [AB: please switch the red and blue colors. The blue colors should always refer to the same waveform model, which is shown in the left panels, otherwise it is very confusing to understand those plots. Please indicate on the figures: GW150914-like and GW190521-like.]

IV. CONSTRAINTS ON QNM FREQUENCIES USING LIGO-VIRGO DATA

[AB: This is the most important section in the paper, because it contains the main results of the paper, i.e., the constraints on QNMs using real data. It needs to be expanded and results would need to be highlighted much better than in the current version. I would like to suggest that besides the Table and the figure with the 2D- and 1D-posteriors that you made (which can be contrasted with Fig. 14 of the TGR GWTC-2 paper), we could have a new figure that is either a combination of Figs. 5 and 6 or only Fig. 5 of the TGR GWTC-2, but for the 22 QNM frequencies for the different GW events. Figures can be used in talks, and can capture the information much better than a list of numbers in a Table.]

The LIGO-Virgo Collaboration recently released their testing GR catalogue containing results ~~of this test~~ for all events observed during O3a [48], which passed a threshold for the total (source-frame) mass $\geq 50M_\odot$ and SNRs in the pre- and post-merger regions ≥ 8.The pre- and post-merger regions of the signal are identified ~~as~~ from the signal's power ~~in the frequency content of the signal~~ before and after the signal reaches the peak's amplitude, ~~as~~ which is determined by the maximum of the likelihood function from the parameter-estimation analysis ~~template~~. [AB: What does it mean "for the purpose of Ref."? We are using present tense in the entire paper, except perhaps the Conclusions section.] For the purpose of Ref. [48], we use~~d~~ a mass threshold and restrict~~ed~~ ourselves to the highest-mass events which ~~were~~ are expected to be most promising to study merger-ringdown. However, since our method relies on doing a parameter estimation on the entire inspiral-merger-ringdown signal, we require the SNR to be beyond a certain threshold throughout the signal for reliable parameter estimation of the initial and final quantities. [AB: there are not "initial" and "final" parameters, there are

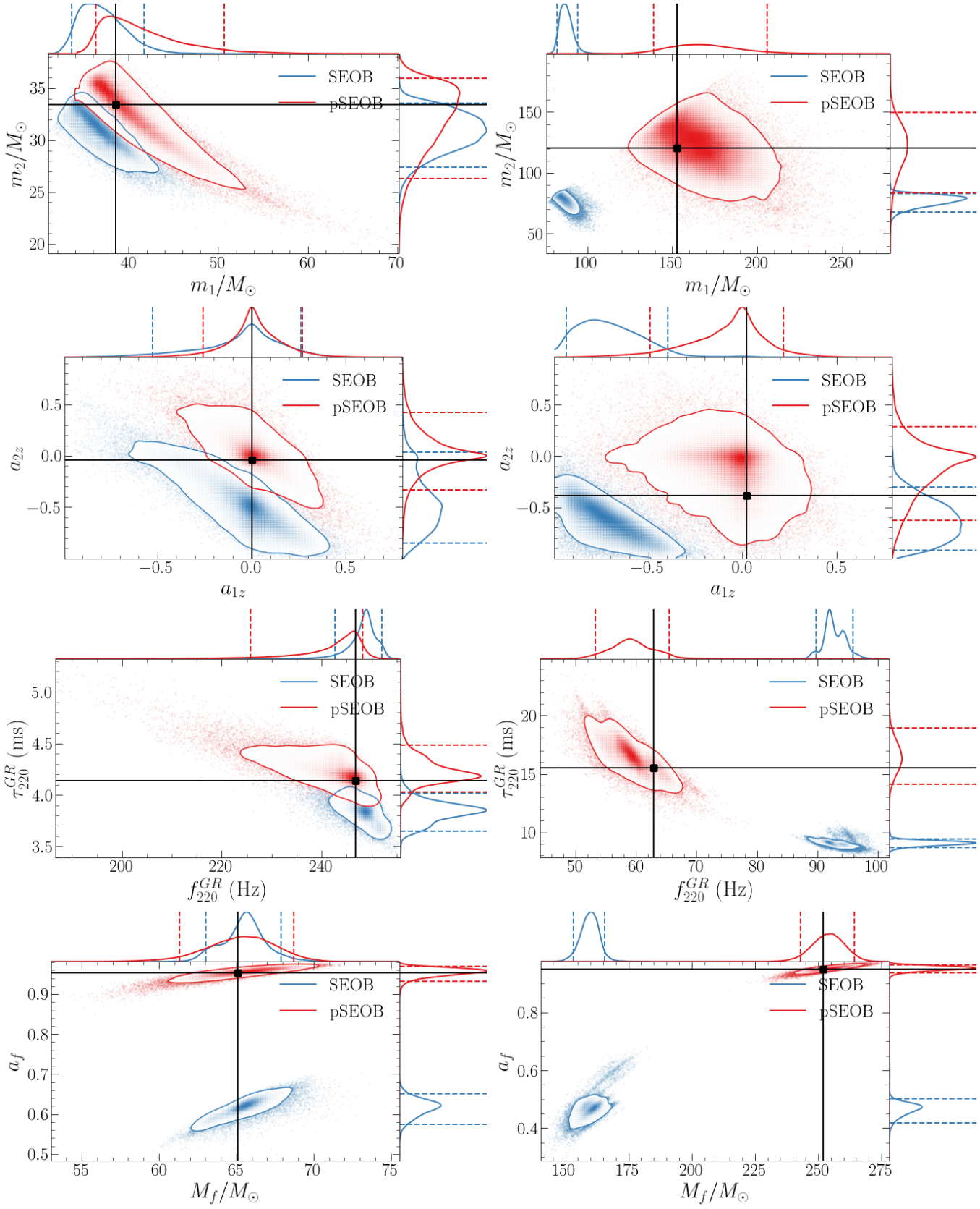

FIG. 4. FINAL RESULT Comparison of ~~the recovered~~ binary's parameters when ~~the underlying signal is assumed to be a GR signal or a modified GR signal~~ a non-GR signal (pSEOBNR) is injected and recovered with a GR (SEOBNR) or a non-GR (pSEOBNR) waveform model. ~~In both cases, the actual underlying signal is a modified GR signal with parameters similar to~~ The left (right) panels refer to a GW150914-like (GW190521- like) injected signal (see Table I) with QNM deviation parameters of $\delta f_{220} = \delta\tau_{220} = 0.5$. ~~For the GW150914 (GW190521) contours, the *SEOB* and *pSEOB* recoveries are indicated by blue (red) and pink (grey) curves respectively.~~ The panels (from top to bottom) show the recoveries in (detector-frame) ~~initial~~ masses (first row), ~~z-components of dimensionless initial~~ (dimensionless) spins (second row), GR predictions of frequency and damping time (third row) and the remnant mass and spin predictions (M_f, a_f) from the frequency and damping time (obtained by inverting the Berti fits). [AB: I would write those details about the "Berti's fits, etc." in the text, not in the caption. Also please specify if the remnant mass is the detector-frame mass. Please switch the red and blue colors. The blue colors should always refer to the same waveform model, i.e., pSEOBNR. Please indicate on the figures: GW150914-like and GW190521-like.]

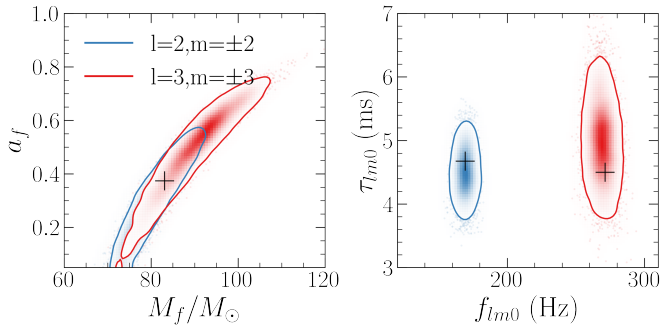

FIG. 5. PRELIMINARY Posterior probability distribution on the fractional deviations (left panel) and the reconstructed (right panel) frequency and damping time of the $(2, \pm 2)$ (blue curves) and $(3, \pm 3)$ (red curves) QNM, respectively, ~~for a numerical relativity signal corresponding to a BBH merger of~~ when a NR signal with parameters $q = 6$, $M = 84 M_\odot$ and SNR = 75 is injected in Gaussian noise and recovered with the pSEOBNR waveform model. The plus signs mark the GR predictions.

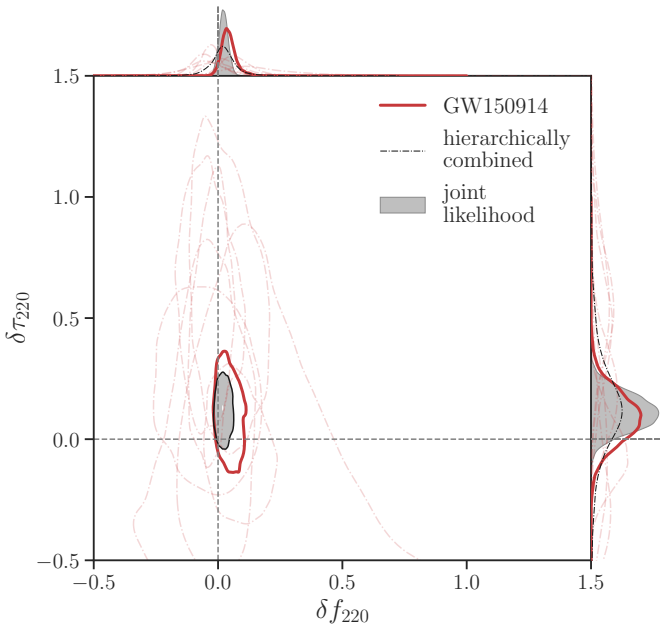

FIG. 6. PRELIMINARY RESULT The 90% credible levels of the posterior probability distribution of the fractional deviations in the frequency and damping time of the $(2, \pm 2)$ QNM, $(\delta f_{220}, \delta\tau_{220})$ and their corresponding one-dimensional marginalized posterior distributions, for events from O1, O2 and O3a passing a SNR threshold of 8 in both the pre- and post-merger signal. The solid red curve marks the best single-event constraint, GW150914, whereas the constraints from the other events are indicated by the dash-dot curves. The joint constraints on $(\delta f_{220}, \delta\tau_{220})$ obtained multiplying the likelihoods from individual events is given by the filled grey contours, while the hierarchical method of combination yields the black dot dashed curves.

the component masses of the holes in the binary, and the mass of the remnant formed after merger.] In fact the SNR threshold alone should be sufficient for the analysis, and for this paper we have relaxed the mass threshold. This has added two events, GW190630_185205 and GW190828_063405, to the list of GW events considered in [48] [*AG: Runs ongoing and looking promising*]. Fig. 6 shows results from these two events along with GW190519_153544, GW190521_074359, GW190910_112807. [AB: Please improve the above paragraph and make it clearer which choice is made for the SNR threshold and masses, and why.]

Furthermore, for the first time, in this paper, we apply our method to measure the QNMs to ~~present results on~~ the relevant GW events from LIGO-Virgo's O1 and O2 runs, alongside the above events. Applying the same thresholds as above, we find three additional events that could be included in the analysis: GW150914, GW170104, GW170729. The other high-mass events from O1-O2, GW170809, GW170814, GW170818 and GW170823 do not have an SNR of 8 in the merger-ringdown signal. For the three relevant signals, GW150914, GW170104 and GW170729, we ~~provide~~ show the posterior distributions in $(\delta f_{220}, \delta\tau_{220})$ in Fig. 6. We also reconstruct the ~~effective~~ QNM parameters, (f_{220}, τ_{220}) which are tabulated in Table II [1] Among all the GW signals detected so far, GW150914 (solid curve in Fig. 6) is unique in its loudness, ~~mass as well as the clarity of the signal,~~ [AB: what is the "clarity" of a signal?] leading to the first, and to date, best attempt in measuring the QNM frequencies [].

Finally, if we assume that the fractional deviations $(\delta f_{220}, \delta\tau_{220})$ take the same values in multiple events, we can assume the posterior of one event to be the prior for the next, and obtain a joint posterior probability distribution. For N observations, where $P_j(\delta f_{220}, \delta\tau_{220}|d_j)$ is the posterior for the j-th observation corresponding to the data set d_j, $j = 1, \ldots, N$, the joint posterior is given by:

$$P(\delta f_{220}, \delta\tau_{220}|\{d_j\}) = P(\delta f_{220}, \delta\tau_{220}) \prod_{j=1}^{N} \frac{P(\delta f_{220}, \delta\tau_{220}|d_j)}{P(\delta f_{220}, \delta\tau_{220})} \tag{4.1}$$

where $P(\delta f_{220}, \delta\tau_{220})$ is the prior on $(\delta f_{220}, \delta\tau_{220})$. However, since we assume the prior on $(\delta f_{220}, \delta\tau_{220})$ to be flat (or uniform), the joint posterior is equal to the joint likelihood.

We show these joint likelihoods on $(\delta f_{220}, \delta\tau_{220})$, as well as, the corresponding 1D marginalized distributions as filled grey curves in Fig. 6. These are the strongest constraints on possible deviations in the measurement of $(\delta f_{220}, \delta\tau_{220})$ to date using our method.[AG: add text on the hierarchical analysis if we want to include that analysis. AB: we want to include that analysis.]

[AB: Please write in the text (equations) the results for $(\delta f_{220}, \delta\tau_{220})$ for GW150914, the joint likelihood and the hi-

[1] See Table IV of Ref. [48] for a list of the SNR thresholds. The paper quotes them for the purpose of the IMR consistency test, but the same thresholds have been used for the *pSEOB* test, as well.

Event	Redshifted frequency [Hz]		Redshifted damping time [ms]	
	IMR	pSEOBNR	IMR	pSEOBNR
GW150914	249^{+9}_{-7}	–	$4.1^{+0.3}_{-0.2}$	–
GW170104	286^{+16}_{-27}	–	$3.5^{+0.4}_{-0.3}$	–
GW170729	161^{+13}_{-14}	–	$7.8^{+1.8}_{-1.5}$	–
GW190630_185205	–	–	–	–
GW190828_063405	–	–	–	–

TABLE II. NOT COMPLETE [AB: We would need to give also the final mass and spins. I would suggest that we list in the Table also the results from the TGR GWTC-2 paper, obtained with our method, so that all the results are in one Table.]

erarchically combined methods.]

V. DISCUSSION

[AB: I am sorry, but I had no time to write this section. Please write a first draft. I have read in the last week several papers about extracting information on the nature of dark objects and gravity in the strong-field regime combining LIGO/Virgo and also EHT. I wanted to refer to them — for example Maggio et al., Volkel et al., Franciolini et al., Cano et al. It is also good if we cite papers that have predicted QNMs in gravity theories alternative to GR. We did it in the paper with Richard and Vivien.]

ACKNOWLEDGEMENTS

LIGO Clusters. [AB: Our cluster!!!] R.B. acknowledges financial support from the European Union's Horizon 2020 research and innovation programme under the Marie Skłodowska-Curie grant agreement No. 792862. This research was supported by the Amaldi Research Center funded by the MIUR program "Dipartimento di Eccellenza" (CUP: B81I18001170001).

Appendix A: Study of systematics on ringdown measurements in real , non-Gaussian noise

[AB: Please improve considerably this Appendix because it is not easy to follow the motivation and the logic. It is written for LIGO people. I have tried to make changes but it is better if you do it. I risk to erase parts that you would consider important. Please write it thinking that your reader is not an LSC reader!]

In Sec. I, we discussed ~~mentioned that~~ the expression of the Bayesian likelihood function that we use in our analysis ~~outlined in~~ (see Eq. 2.12) and stressed that it~~and 2.13~~ is only valid if the interferometric noise can be described as a stationary Gaussian process. LIGO-Virgo noise, however, frequently has non-stationary and/or non-Gaussian features, for example glitches, which can affect parameter inferences unless appropriately accounted for. Here we demonstrate, by injecting in real noise a GW190521-like signal ~~with an example of a GW190521-like simulated signal~~, how systematic biases can originate ~~likely originating~~ from an incomplete understanding of the noise. [AB: It is confusing to refer to "systematic" biases for the noise, generally we refer to systematic biases for the waveform modeling. In fact, below you also, somewhat suddenly, refer to (lack of) precession, as a possible source of systemtcis. I would advice you to clarify from the beginning of this Appendix, what this study is about and what you intend to do below.]

The spinning, precessing NR-surrogate model `NRSur7dq4`,

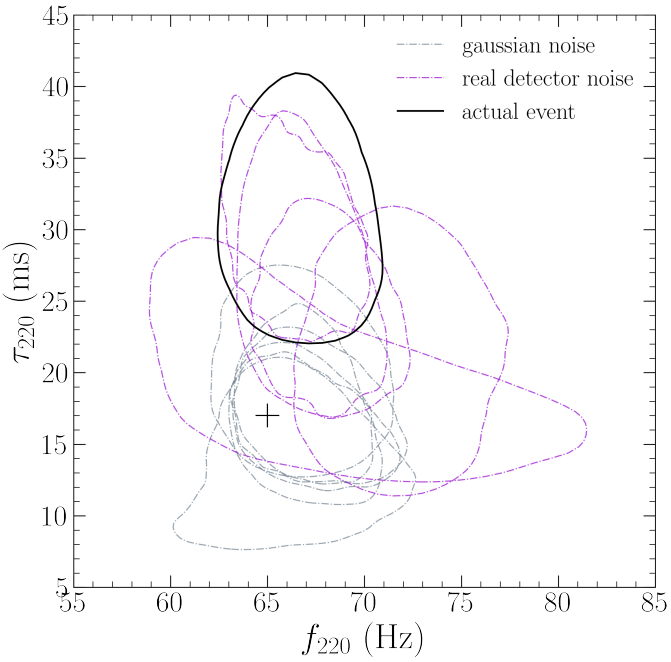

FIG. 7. FINAL RESULT 90 % credible level on the posterior probability distribution of the frequency and damping time of $(2,\pm2)$ mode, $(f_{220}^{\rm GR}, \tau_{220}^{\rm GR})$ from simulations [AB: I have changed this in other places. The word "simulations" is confusing, because we deal with a paper in which we also refer to NR simulations. I suggest to use "injected synthetic signals" instead] of an `NRSur7dq4` GW signal with parameters similar to the GW event, GW190521, in Gaussian noise (grey dot-dashed lines) and real interferometric noise (pink dot dashed lines). The GR prediction for the frequency and damping time is indicated by the black cross. While the Gaussian noise simulations are consistent with the prediction, at least 3 or the 5 real noise simulation are not. For comparison, we also plot the 90 % credible level for the actual event, GW190521. [AB: For clarity, please indicate on the plot which waveform model is used to obtain such posteriors, as you did in the other plots of the paper. Also, please use something else instead of "actual event", which is confusing. The problem is that the first two entries of the legend refer to the noise properties of the PE study done with an injected synthetic signal, whereas I believe "actual event" refers to "real" not injected signal and "real noise". All the entries in the legend need to be consistent with each other; you need to specify for each of them the "signal" and the "noise". I hope is clear what I am saying]

valid up to mass ratio 4, was employed (together with the SEOBNR model) to analyze the GW190521 signal observed by the LIGO and Virgo detectors. For the injected synthetic signal we use a NRSur7dq4 waveform with parameters similar to the ones recovered by this model on the actual GW190521 data (see Table I of Ref. [49]). In Fig. 7, we indicate with a black cross what the injected NRSur7dq4 signal predicts for the $(2,2)$ frequency and damping time, and for comparison, we also show with a black solid curve the results obtained when recovering the the actual signal GW190521 with the waveform model pSEOBNR. As seen in the plot, while the measurement of the frequency is consistent with the prediction, we overestimate the damping time. [AB: it is not clear to me what the figure shows. Is the black line the result when running pSEOBNR against real data or the injection in realt data?]

[AB: What is the "underlying" NR signal? I think you are referring to the injected signal. Also, until now you have not discussed precession.] The underlying NR signal is expected to be precessing, and since the pSEOBNR model is built on an aligned-spin GR model, a lack of precession could bias measurements. We explore effects of possible waveform systematics by injecting the signal is coloured Gaussian noise. In this case, since the understanding of the noise realizations is complete, any measurement biases could only arise from incomplete understanding of the ~~underlying~~ injected signal. We find (grey curves in Fig.7) our results to be consistent with the prediction thus ruling out a lack of precession to be a likely cause for the bias in the damping time measurement of the actual signal.

We subsequently study the effects of possible noise systematics by injecting the same NRSur7dq4 GW signal in different realizations of actual interferometric noise around the real event GW190521. Since the PSDs of the GW detectors are expected to vary over longer durations of time, we select 5 different noise realizations over a segment of 2.5 hours of coincident data in both the LIGO detectors centered at the time of the actual event. The noise properties in this chunk of data, and consequently for all 5 simulated signals, is expected to be the closest to that for the actual event. The results are indicated by ~~pink~~ green curves in Fig. 7. As it can be seen from the figure, for 3 of the 5 noise realizations, corresponding to $t_0 - 1$ hour, $t_0 + 0.5$ hours, and $t_0 + 1$ hour we recover a damping time similar to the actual event, where t_0 is the GPS time of the actual event. For the other two noise realizations, we estimate the consistent damping time but an off-set frequency, while the fifth noise realization is consistent with both predictions. The SNR in the Livingston detector goes down by more than a factor 3 in some runs, indicative of how a variation in the noise strongly affects our ability to infer parameters. This also seems to indicate that a bias in the measurements of the damping time for the actual event [AB: not clear what you mean] can be unaccounted noise systematics.

[1] *LIGO scientific collaboration*, https://www.ligo.org/.

[2] *Virgo collaboration*, https://www.virgo-gw.eu/.

[3] B. Abbott, R. Abbott, T. Abbott, S. Abraham, F. Acernese, K. Ackley, C. Adams, R. Adhikari, V. Adya, C. Affeldt, et al., Physical Review X **9**, 031040 (2019).

[4] J. Aasi, J. Abadie, B. Abbott, R. Abbott, T. Abbott, M. Abernathy, T. Accadia, F. Acernese, C. Adams, T. Adams, et al., Classical and Quantum Gravity **32**, 115012 (2015).

[5] F. Acernese, M. Agathos, K. Agatsuma, D. Aisa, N. Allemandou, A. Allocca, J. Amarni, P. Astone, G. Balestri, G. Ballardin, et al., Classical and Quantum Gravity **32**, 024001 (2014).

[6] A. H. Nitz, C. Capano, A. B. Nielsen, S. Reyes, R. White, D. A. Brown, and B. Krishnan, The Astrophysical Journal **872**, 195 (2019).

[7] A. H. Nitz, T. Dent, G. S. Davies, S. Kumar, C. D. Capano, I. Harry, S. Mozzon, L. Nuttall, A. Lundgren, and M. Tápai, The Astrophysical Journal **891**, 123 (2020).

[8] B. Zackay, T. Venumadhav, L. Dai, J. Roulet, and M. Zaldarriaga, Phys. Rev. D **100**, 023007 (2019), 1902.10331.

[9] T. Venumadhav, B. Zackay, J. Roulet, L. Dai, and M. Zaldarriaga, Phys. Rev. D **101**, 083030 (2020), 1904.07214.

[10] T. Venumadhav, B. Zackay, J. Roulet, L. Dai, and M. Zaldarriaga, Physical Review D **101** (2020), ISSN 2470-0029, URL http://dx.doi.org/10.1103/PhysRevD.101.083030.

[11] B. P. Abbott, R. Abbott, T. Abbott, M. Abernathy, F. Acernese, K. Ackley, C. Adams, T. Adams, P. Addesso, R. Adhikari, et al., Physical review letters **116**, 061102 (2016).

[12] B. P. Abbott et al. (LIGO Scientific Collaboration), The Astrophysical Journal Letters **818**, L22 (2016), 1602.03846.

[13] B. P. Abbott, R. Abbott, T. D. Abbott, F. Acernese, K. Ackley, C. Adams, T. Adams, P. Addesso, R. X. Adhikari, V. B. Adya, et al., The Astrophysical Journal **848**, L12 (2017), ISSN 2041-8213, URL http://dx.doi.org/10.3847/2041-8213/aa91c9.

[14] B. P. Abbott, R. Abbott, T. D. Abbott, F. Acernese, K. Ackley, C. Adams, T. Adams, P. Addesso, R. X. Adhikari, V. B. Adya, et al., The Astrophysical Journal **848**, L13 (2017), ISSN 2041-8213, URL http://dx.doi.org/10.3847/2041-8213/aa920c.

[15] Nature **551**, 8588 (2017), ISSN 1476-4687, URL http://dx.doi.org/10.1038/nature24471.

[16] B. P. Abbott et al. (LIGO Scientific and Virgo Collaborations), Phys. Rev. Lett. **116**, 221101 (2016), URL http://link.aps.org/doi/10.1103/PhysRevLett.116.221101.

[17] B. Abbott, R. Abbott, T. Abbott, F. Acernese, K. Ackley, C. Adams, T. Adams, P. Addesso, R. Adhikari, V. Adya, et al., Physical Review Letters **123** (2019), ISSN 1079-7114, URL http://dx.doi.org/10.1103/PhysRevLett.123.011102.

[18] B. Abbott, R. Abbott, T. Abbott, S. Abraham, F. Acernese, K. Ackley, C. Adams, R. Adhikari, V. Adya, C. Affeldt, et al., Physical Review D **100** (2019), ISSN 2470-0029, URL http://dx.doi.org/10.1103/PhysRevD.100.104036.

[19] B. P. Abbott et al. (LIGO Scientific and Virgo Collaboration), Phys. Rev. Lett. **118**, 221101 (2017), URL https://link.aps.org/doi/10.1103/PhysRevLett.118.221101.

[20] A. Samajdar and K. Arun, Physical Review D **96**, 104027 (2017).

[21] B. P. Abbott et al. (LIGO Scientific Collaboration and Virgo Collaboration), Phys. Rev. Lett. **119**, 141101 (2017), URL https://link.aps.org/doi/10.1103/PhysRevLett.119.141101.

[22] M. Isi and A. J. Weinstein, arXiv preprint arXiv:1710.03794 (2017).

[23] A. Ghosh et al., Phys. Rev. D **94**, 021101(R) (2016), 1602.02453.

[24] A. Ghosh, N. K. Johnson-Mcdaniel, A. Ghosh, C. K. Mishra, P. Ajith, W. Del Pozzo, C. P. Berry, A. B. Nielsen, and L. London, Class. Quant. Grav. **35**, 014002 (2018), 1704.06784.

[25] S. Ghonge, K. Chatziioannou, J. A. Clark, T. Littenberg, M. Millhouse, L. Cadonati, and N. Cornish (2020), 2003.09456.

[26] R. Brito, A. Buonanno, and V. Raymond, Phys. Rev. D **98**, 084038 (2018), 1805.00293.

[27] M. Giesler, M. Isi, M. A. Scheel, and S. Teukolsky, Phys. Rev. X **9**, 041060 (2019), 1903.08284.

[28] M. Isi, M. Giesler, W. M. Farr, M. A. Scheel, and S. A. Teukolsky, Phys. Rev. Lett. **123**, 111102 (2019), 1905.00869.

[29] S. Bhagwat, X. J. Forteza, P. Pani, and V. Ferrari, Phys. Rev. D **101**, 044033 (2020), 1910.08708.

[30] X. J. Forteza, S. Bhagwat, P. Pani, and V. Ferrari (2020), 2005.03260.

[31] E. Berti, V. Cardoso, and C. M. Will, Phys. Rev. D **73**, 064030 (2006), gr-qc/0512160.

[32] G. Carullo, G. Riemenschneider, K. W. Tsang, A. Nagar, and W. Del Pozzo, Class. Quant. Grav. **36**, 105009 (2019), 1811.08744.

[33] G. Carullo, W. Del Pozzo, and J. Veitch, Phys. Rev. D **99**, 123029 (2019), [Erratum: Phys.Rev.D 100, 089903 (2019)], 1902.07527.

[34] S. Bhagwat, M. Cabero, C. D. Capano, B. Krishnan, and D. A. Brown (2019), 1910.13203.

[35] M. Cabero, C. D. Capano, O. Fischer-Birnholtz, B. Krishnan, A. B. Nielsen, A. H. Nitz, and C. M. Biwer, Phys. Rev. D **97**, 124069 (2018), 1711.09073.

[36] A. B. Nielsen, C. D. Capano, O. Birnholtz, and J. Westerweck, Phys. Rev. D **99**, 104012 (2019), 1811.04904.

[37] K. W. Tsang, A. Ghosh, A. Samajdar, K. Chatziioannou, S. Mastrogiovanni, M. Agathos, and C. Van Den Broeck, Phys. Rev. D **101**, 064012 (2020), 1906.11168.

[38] R. Lo, T. Li, and A. Weinstein, Phys. Rev. D **99**, 084052 (2019), 1811.07431.

[39] J. Abedi and N. Afshordi, JCAP **11**, 010 (2019), 1803.10454.

[40] J. Abedi and N. Afshordi (2020), 2001.00821.

[41] A. Testa and P. Pani, Phys. Rev. D **98**, 044018 (2018), 1806.04253.

[42] S. Bhagwat, M. Okounkova, S. W. Ballmer, D. A. Brown, M. Giesler, M. A. Scheel, and S. A. Teukolsky, Phys. Rev. D **97**, 104065 (2018), 1711.00926.

[43] A. Bohé et al., Phys. Rev. D **95**, 044028 (2017), 1611.03703.

[44] R. Cotesta, A. Buonanno, A. Bohé, A. Taracchini, I. Hinder, and S. Ossokine, Phys. Rev. D **98**, 084028 (2018), 1803.10701.

[45] E. Berti, V. Cardoso, and A. O. Starinets, Class. Quant. Grav. **26**, 163001 (2009), 0905.2975.

[46] A. Taracchini et al., Phys. Rev. D **89**, 061502 (2014), 1311.2544.

[47] F. Hofmann, E. Barausse, and L. Rezzolla, Astrophys. J. Lett. **825**, L19 (2016), 1605.01938.

[48] R. Abbott et al. (LIGO Scientific, Virgo) (2020), 2010.14529.

[49] R. Abbott et al. (LIGO Scientific, Virgo), Phys. Rev. Lett. **125**, 101102 (2020), 2009.01075.